Assessment of biomass burning smoke influence on environmental conditions for multi-year tornado outbreaks by combining aerosol-aware microphysics and fire emission constraints

Pablo E. Saide (1), Gregory Thompson (2), Trude Eidhammer (2), Arlindo M. da Silva (3), R. Bradley Pierce (4) and Gregory R. Carmichael (5)

(1) Advanced Study Program and Atmospheric Chemistry Observations and Modeling Lab, National Center for Atmospheric Research, Boulder, Colorado, USA.

(2) Research Applications Laboratory, National Center for Atmospheric Research, Boulder, Colorado, USA.

(3) Global Modeling and data Assimilation Office, NASA Goddard Space Flight Center, Greenbelt, Maryland, USA.

(4) NOAA Satellite and Information Service (NESDIS) Center for Satellite Applications and Research (STAR), Madison, Wisconsin, USA.

(5) Center for Global & Regional Environmental Research, University of Iowa, Iowa City, Iowa, USA.

Correspondence to: P. E. Saide (saide@ucar.edu)

Key Points

- WRF with aerosol-aware microphysics is used to study smoke impacts on multiple tornado outbreaks

- Although smoke is always present, changes in environmental conditions due to smoke are highly variable
- WRF and WRF-Chem simulations can produce similar AOD and smoke impacts

Abstract

We use the WRF system to study the impacts of biomass burning smoke from Central America on several tornado outbreaks occurring in the US during spring. The model is configured with an aerosol-aware microphysics parameterization capable of resolving aerosol-cloud-radiation interactions in a cost-efficient way for numerical weather prediction (NWP) applications. Primary aerosol emissions are included and smoke emissions are constrained using an inverse modeling technique and satellite-based AOD observations. Simulations turning on and off fire emissions reveal smoke presence in all tornado outbreaks being studied and show an increase in aerosol number concentrations due to smoke. However, the likelihood of occurrence and intensification of tornadoes is higher due to smoke only in cases where cloud droplet number concentration in low level clouds increases considerably in a way that modifies the environmental conditions where the tornadoes are formed (shallower cloud bases and higher low-level wind shear). Smoke absorption and vertical extent also play a role, with smoke absorption at cloud-level tending to burn-off clouds and smoke absorption above clouds resulting in an increased capping inversion. Comparing these and WRF-Chem simulations configured with a more complex representation of aerosol size and composition and different optical properties, microphysics and activation schemes, we find similarities in terms of the simulated aerosol optical depths and aerosol impacts on near-storm environments. This provides reliability on the

aerosol-aware microphysics scheme as a less computationally expensive alternative to WRF-Chem for its use in applications such as NWP and cloud-resolving simulations.

1. Introduction

Numerical weather prediction (NWP) is routinely used by forecasters as a tool (among many others) to warn the population of possible severe weather events and is thought to be at least partially responsible for a decrease in death tolls during tornado outbreaks (Brooks and Doswell, 2002). When building convective outlooks and issuing "Tornado Watches", NWP is generally used to forecast the environmental conditions that are favorable for the formation of tornadoes. These conditions include high low-level wind shear, storm-relative helicity (SRH) and convective-available potential energy (CAPE); and low lifting condensation level (LCL, roughly the cloud base height), which are often combined in composite parameters (e.g., Significant Tornado Parameter (STP)) to provide a combined score (Rasmussen and Blanchard, 1998; Thompson et al., 2003). Recent studies have begun analyzing the influence of large-scale phenomena such as the Madden-Julian Osciallation (Barrett and Gensini, 2013) and climate change (Brooks, 2013; Diffenbaugh et al., 2013) on these precursor atmospheric conditions common to tornado days. The mechanisms through which these environmental conditions are connected to tornado genesis, longevity, and intensity have been hypothesized (Markowski and Richardson, 2009), but remain as open questions. However, as forecasts of these conditions have shown skill on predicting severe weather outbreaks (e.g., Hamill et al., 2005; Knupp et al., 2013), a continuous effort to improve these forecasts further is needed.

63 Aerosols can interact with clouds and solar radiation and modulate climate (Boucher et al.,
64 2013). The inclusion of these interactions into NWP can impact forecasts (e.g., Kolusu et al.,
65 2015). Convective-scale weather prediction models are moving towards the inclusion of these
66 interactions by the use of aerosol-aware microphysics that incorporate aerosols explicitly in a
67 simple and cost-effective manner (Lebo and Morrison, 2013; Thompson and Eidhammer, 2014).
68 More complex schemes that resolve atmospheric chemistry and represent the size and
69 composition distributions of aerosols with greater detail (e.g., Eidhammer et al., 2014) are
70 currently too computationally expensive to be used in operational high-resolution forecasts. A
71 comparison between these two types of schemes could be performed to assess how aerosols may
72 impact specific weather phenomena and how much complexity in aerosol treatment may be
73 warranted for future operational NWP.

74 Biomass burning aerosol (smoke) is estimated to be the major contributor to the global burden of
75 fine carbonaceous aerosols (Andreae and Rosenfeld, 2008; Bond et al., 2004) and to significantly
76 influence climate (Jacobson, 2014). In particular, smoke from fires in Central America has been
77 shown to be in the inflow of severe weather in the US and has been hypothesized to intensify the
78 outbreaks by the convective invigoration mechanism (Wang et al., 2009). Saide et al. (2015b)
79 found that Central American smoke was capable of intensifying tornado outbreaks by lowering
80 LCL and increasing low level shear. This is achieved through two pathways: 1) optical
81 thickening of shallow clouds present before the outbreak which reduce downward solar radiation
82 at the surface stabilizing the boundary layer, and 2) enhancement of the capping inversion by
83 heating of the layer above cloud by soot absorption (Saide et al., 2015b). These studies focused
84 on specific outbreaks and there has been no assessment of these aerosol-associated impacts for
85 multiple outbreaks on multiple years.

This study intends to advance our understanding on the interactions of smoke with severe weather and to help transition the inclusion of fully-coupled aerosol-cloud-radiation interactions into NWP. To do so, we compare simple and complex treatments of these interactions in the Weather Research and Forecasting (WRF) and WRF-Chem systems, explore the influence of smoke presence on tornado outbreaks occurring in multiple years, and evaluate the relevance of the proposed mechanism proposed in Saide et al. (2015b) in these outbreaks (Section 3). Furthermore, biomass burning emissions have been found to have large uncertainties; for instance, Kaiser et al. (2012) found that a factor of three increase in smoke emissions is needed to improve agreement with observations, while Zhang et al. (2014) found discrepancies of up to a factor of 10 between various smoke emission estimates. Thus, to reduce these uncertainties, in this study biomass burning emissions are constrained for each outbreak with satellite-based aerosol optical depth (AOD) retrievals using a recently developed algorithm (Saide et al., 2015a). The next section describes details on the tornado outbreaks studied, the modeling framework and the inversion algorithm. Section 3 contains results and discussion about the emission inversions and smoke presence and impacts during outbreaks, while in the last section we provide conclusions and future directions.

2. Methods

2.1. Tornado Outbreaks studied

We selected eight major tornado outbreaks between 2003 and 2014. This period was chosen due to availability of data from the Moderate Resolution Imaging Spectroradiometer (MODIS) on both Terra and Aqua satellites (operational from mid-2002 to date) as fire emissions and AOD retrievals used herein are based on the MODIS products (see next sections). Only episodes

occurring during April and May (not including those very early and very late in each month, respectively) were chosen to coincide with the strongest biomass burning in Central America (Reid et al., 2004). The tornado tracks of the outbreaks selected are shown in Figure 1 and represent locations across the Southeast, Midwest and Southwest United States (US). Other selection criteria were for each outbreak to contain at least four tornadoes of EF2 scale or greater (to filter out the less significant outbreaks), the tornados were not so broadly spread in order that model simulations would fit reasonably within a nested domain, and the most severe and more numerous tornadoes needed to occur in the afternoon or early evening. The latter condition is imposed because the proposed mechanisms being studied are driven by peak solar heating, which would dissipate at night or not yet occur in the morning. Many of these outbreaks have been highlighted as major events of the year they occurred (Blunden and Arndt, 2012, 2014, 2015; Levinson and Lawrimore, 2008; Levinson and Waple, 2004; Peterson and Baringer, 2009) and specific studies have focused on their characteristics and impacts (Hamill et al., 2005; Knupp et al., 2013). The environmental conditions provided by Storm Prediction Center (SPC) Convective Outlooks and Mesoscale Analysis for these outbreaks are shown in Figure 2.

2.2. Regional modeling

We use two configurations of the WRF system to perform simulations of aerosols and their impacts on weather, one with the Thompson and Eidhammer (2014; hereafter referred to as TE2014) aerosol-aware microphysics (AAM) scheme and the other with WRF-Chem.

The TE2014 aerosol-aware microphysics consists of a double-moment bulk microphysical parameterization that explicitly resolves droplet nucleation and ice activation due to aerosols. Besides cloud water, cloud ice, snow, graupel, and rain hydrometeor species, the scheme

transports two aerosol species (hygroscopic and ice-nucleating) adding only about 15% computational cost, therefore making it suitable for NWP applications. Aerosol-radiation interactions were recently included to the AAM configuration by computing AOD at 550 nm based on the two aerosol species using a look-up table procedure to include aerosol hygroscopic growth. Then, spectral AOD and other aerosol optical properties (AOPs) such as Angstrom exponent, single-scattering albedo and asymmetry factor are parameterized following the methods of Ruiz-Arias et al. (2014) considering a rural type aerosol. These spectral AOPs are then used in the Rapid Radiative Transfer Model for climate and weather models (RRTMG) shortwave radiation parameterization (Iacono et al., 2008).

While TE2014 used a constant flux derived from initial aerosol concentrations to represent emission processes, we modified WRF-Chem emission routines to include primary-aerosol number emissions explicitly into the aerosol-aware microphysics parameterization. The MOSAIC aerosol scheme (Zaveri et al., 2008) in WRF-Chem can solve aerosol mass and number for 8 sectional size bins. Thus, emission routines coupled to this scheme (anthropogenic, fires, dust and sea-salt) provide aerosol number per size bin, which were summed up to obtain total aerosol number concentrations needed by the TE2014 scheme. We used biomass burning emissions produced by the Quick Fire Emission Dataset (QFED) v2.4 (Darmenov and da Silva, 2015) which were included into the model using the WRF-Chem online plume rise model (Grell et al., 2011). Anthropogenic emissions correspond to NEI 2005 (http://www.epa.gov/ttnchie1/net/2005inventory.html) for the US, 1999 Mexico emissions described in Mena-Carrasco et al. (2009) updated to 2012 using growth factors from Wolf et al. (2009), and emissions derived with PREP-CHEM-SRC code (Freitas et al., 2011) for the rest of Central America. Sea-salt and dust emissions were estimated online by using the Gong et al.,

(1997) and Zhao et al. (2010) parameterizations, respectively. Although secondary aerosol production is not modeled (no chemical mechanism used and no gaseous species modeled), it should not affect aerosol number concentration significantly as secondary aerosol is expected to condense on already existing particles. Aerosol boundary conditions are provided every 6 hours by global simulations of MOZART (Emmons et al., 2010), while initial conditions are obtained from the monthly climatology derived by Thompson and Eidhammer (2014). The month when the simulation was started was used as initial condition when fire emissions were included, while February was used for simulations without fire emissions to provide a smoke-free initialization. As in TE2014, only dust was considered to be ice nucleating while all other aerosol species (except black carbon) were apportioned to the hygroscopic aerosol. Although black carbon is not apportioned, the two aerosol species are considered to absorb solar radiation as mentioned above.

WRF-AAM was configured for each tornado outbreak by using two domains of 12 km and 4 km grid-spacing. The outer domains covered roughly between -110° and -75° longitude for all outbreaks, and from 10° to 50° latitude for outbreaks in 2007 and 24 May 2008 and from 10° to 45° latitude for the rest of the outbreaks (Fig. 3). The inner domains are shown in Figure 1 and were designed to include each outbreak region. All simulations were initialized at 00 UTC seven days prior to the outbreak studied to provide spin-up time for aerosol concentration and feedbacks to meteorology. Meteorological initial and boundary conditions were obtained from NCEP final analysis (NCEP, 2000). Other WRF configuration choices include RRTMG long-wave radiation (Iacono et al., 2000), MYJ boundary layer (Janjić, 2002), Noah land surface model (Barlage et al., 2010), GF cumulus scheme (Grell and Freitas, 2013) for the 12 km domain and no convective parameterization was used for the 4 km domain. Figure 2 compared to Figure 4 shows that the model configured this way is able to represent the tornadic environment found

176 on all outbreaks, although some shifts in the maximum values are often found which is expected
177 due to the long spin-up used.

178 The WRF-Chem configuration used is the same as the one described in Saide et al. (2015b)
179 unless noted differently here. For consistency between simulations, WRF-Chem uses the same
180 configuration as WRF-AMM, including domains, vertical and horizontal resolution, emission
181 databases, initial and boundary conditions, and physics configuration, excluding the
182 microphysics and aerosol activation parameterizations where the Morrison and Abdull-Razak
183 and Ghan schemes are used (Abdul-Razzak and Ghan, 2002; Yang et al., 2011 and references
184 therein). The chemical mechanism and aerosol models correspond to the CBMZ (Zaveri and
185 Peters, 1999) and 8 size bin MOSAIC (Zaveri et al., 2008).

186 2.3. Inversion scheme

187 The algorithm described in Saide et al. (2015a) is used to constrain biomass burning emissions
188 for each outbreak studied. The algorithm requires the use of two WRF simulations, one with
189 first-guess (or initial) emissions (QFED in this case) and another one with perturbed emissions.
190 As assessing smoke impacts involves performing simulations with and without fire emissions
191 (Saide et al., 2015b), the perturbed simulation is chosen as the one with the fire emissions turned
192 off (i.e., perturbation factor equals zero). This reduces the computational burden because the
193 perturbation simulation is used both for the inversion step and for assessing the smoke effects.
194 Also, the simulations need to produce estimates of the observation used to constrain emissions,
195 which in this case is AOD and can indeed be estimated by WRF-AAM (see previous section).
196 Additionally, the simulations used in the inversion algorithm need to solve for tracers tagged to
197 the emissions being constrained. These tracers provide the emission's footprint in the

198 observation location and are used to derive the sensitivities (derivatives) used in the inversion
199 scheme. In this study the tracers are tagged to fire emissions from four regions, every six hours
200 and during eight day simulations, resulting in 128 tracers. The four regions are shown in Figure 5
201 and correspond roughly to the east (1) and west (2) of the Mexican Central Plateau, (3) the
202 Yucatan peninsula including Belize and Guatemala, and (4) the rest of Central American
203 countries to the south. The tracers are modeled only on the 12 km domain as here is where the
204 inversion is performed.

205 The variational inversion algorithm determines the optimal scaling factors to be applied to the
206 fire emissions. A cost function with two terms is minimized to (1) improve model fit to the
207 observations but at the same time (2) do not exceedingly deviate from the initial guess estimate.
208 We use the same parameters as in Saide et al. (2015a) to weight these two terms with the
209 exception of the length scale to correlate emissions temporally, which is changed from 4 to 6
210 hours. This choice of parameters provides a good fit to the data with little bias and produces
211 large deviations from the highly uncertain guess emissions, but does not generate very steep
212 temporal changes in the correction factors. Finally, one more simulation is performed with the
213 constrained emissions, and this simulation is compared to the one without fire emissions to
214 assess the smoke impacts. These two simulations (constrained fire emissions and no fires) use
215 the two domains (12 km and 4km resolution) and comparisons are performed on the inner
216 domain only. The inversions are performed only for the WRF-AAM configurations, while WRF-
217 Chem configurations using constrained smoke emissions use the ones obtained from WRF-AAM
218 inversions corresponding to the same episode.

219 We use observed AOD at 550 nm from the NASA neural-network retrieval (NNR, GMAO,
220 2014; Saide et al., 2013) to constrain emissions, which are assimilation-grade retrievals based on

MODIS products calibrated to match Aerosol RObotic NETwork (AERONET) AOD data (Holben et al., 2001). Only NNR observations from -110° to -80° longitude, from 10° to 30° latitude, and over 0.2 AOD are used in the inversion to avoid correcting fire emissions based on retrievals far from the source region and not significantly influenced by fires.

2.4. Summary of simulations

We performed three WRF-AAM simulations for the eight outbreaks studied: 1) Fire emissions turned off and two domains, 2) Initial fire emissions including tracers and only for the 12km domain, and 3) Constrained emissions for the two domains. These sum up to 24 simulations. Then, we performed various sensitivity simulations by turning off absorption and changing initial smoke emissions (see section 3.4 for details) for three outbreaks. One simulation per outbreak was performed for absorption effects (only #3 as fire off was already performed), while two for the initial emissions sensitivity (#2 and #3 as the inversion needs to be repeated). Together with the base-line simulations, this gives a total of 33 WRF-AAM simulations. We also performed simulations #1 and #3 using WRF-Chem for three outbreaks, thus a total of 6 WRF-Chem simulations (section 3.5). Additionally, one WRF-Chem simulation of type #2 but without the tracers was performed to compare AOD against WRF-AAM. Note that each WRF-Chem simulation is ~10 times more computationally expensive than the corresponding WRF-AAM.

3. Results and discussion

3.1. Inversion results

Figure 5 shows the daily emissions by region before and after the inversion for all outbreaks studied when using the AAM configuration. Prior smoke emissions are found to be underestimated for most times during all cases studied, with domain-wide emission scaling

243 factors in the range of 1.4-2.6, depending on the case. The corrections to the prior emissions tend
244 to vary substantially by region and by day, which shows that the choice of independently
245 constraining emissions by region and by time was appropriate. Figure 6 shows an example of
246 how the modeled AOD generally improves the fit with respect to the observations after
247 constraining emissions, indicating that the inversion algorithm is functioning properly. Although
248 there is overall improvement, some regions show degraded AOD after the inversion (e.g.,
249 southwest Mexico), which can happen because of the limited number of parameters being
250 optimized (4 regions, 4 times a day) and the large amount of data being ingested (i.e., the system
251 is over determined).

252 3.2. Smoke presence within outbreak regions

253 Figure 7 (top panels) shows the vertical distributions of aerosol number concentration in the
254 region of each outbreak studied, while Figure 8 shows the boundary layer height distributions.
255 We find that smoke contributes significantly to the total aerosol number concentration for all of
256 the outbreaks analyzed no matter the location of the outbreak. Smoke can be effectively
257 transported to the regions where outbreaks occur due to the southerly airflow from the Gulf of
258 Mexico during spring (Wang et al., 2006; Wang et al., 2009) and because of the low-level jet that
259 transports warm, moist air from the same region, which is a typical feature that triggers these
260 outbreaks (Hamill et al., 2005; Knupp et al., 2013). The vertical location of smoke can vary from
261 case to case; with all outbreaks showing smoke within the boundary layer and only some cases
262 (15 and 27 April 2011, 28 April 2014) presenting a thick smoke layer extending higher into the
263 lower troposphere (up to ~5 km). WRF-Chem simulations for the 27 April 2011 outbreak also
264 showed a thick layer of smoke (Saide et al., 2015b), which is consistent with the WRF-AAM
265 results and as expected because both model configurations use the same transport scheme.

CALIPSO provides observations of vertically resolved aerosols, which can be used to evaluate the modeled vertical distribution of the smoke layer when the satellite overpasses it. Since the regions where the outbreaks occur are generally cloudy, we performed the evaluation over the Gulf of Mexico, which is the inflow region (Figure 3). We find the model generally reproduces the layers observed by CALIPSO with skill and at a similar altitude, going from shallow layers of smoke found on 28 April 2014 to layers up to ~6 km altitude on 15 April 2011. This shows that the plume rise parameterization and the model transport are reliable, which increases the confidence on the vertical distribution of smoke on the outbreaks regions shown on Figure 7.

3.3. Impacts on environmental conditions

The changes produced by the presence of smoke in near-storm environment conditions can be obtained by comparing simulations with and without smoke emissions (Figure 9). Although smoke is present in the outbreak region for all cases studied, the impacts of smoke on environmental conditions vary by case. The outbreaks on 4 May 2003 and 27 April 2011 show the largest and most consistent effects of smoke on LCL (~90-130 m reduction in mean), low-level shear (1.5-2.2 m/s increase in mean) and SRH (30-80 m^2/s^2 increase in mean), with the interquartile region showing values that produce an intensification of tornadic environments (negative LCL and positive 1-km shear and SRH differences). Statistics of these variables for multiple events have shown that differences in median between supercell types (non-tornadic to weakly tornadic, and weakly to significantly tornadic) are ~-170 m, 1.7 m/s and ~30-45 m^2/s^2 for LCL, low-level shear and SRH, respectively (Thompson et al., 2003). Thus, the smoke effects shown here can reach magnitudes relevant for tornadogenesis and increase in tornado intensity.

Given that the statistics in Figure 9 are computed using a large number of grid-cells (7,000-23,000 depending on the case), statistically significant differences are likely to be found even if differences between simulations are small. Thus, instead of using *p-values*, we estimate the magnitude of the difference between groups (effect size) using the standardized difference (difference between means divided by the standard deviation of either group) and consider small, medium, large, and very large values of this quantity equal to 0.2, 0.5, 0.8 and 1.3, respectively (Sullivan and Feinn, 2012). As expected, the outbreaks on 4 May 2003 and 27 April 2011 show medium to large effect size for LCL, 1km shear and SRH (Figure 9). While 10 May 2008, 15 April 2011 and 28 April 2014 generally show a small effect size, the rest of the outbreaks show negligible effects of smoke. Although the 23 May 2008 and 19 May 2013 outbreaks show positive LCL mean (i.e., a reduction in tornado likelihood due to smoke), this is found to be a negligible effect size due to the large spread in these simulations.

Elevated CAPE and large-scale shear (6 km layer) are generally understood as a requirement for supercell formation rather than an indicator to discriminate between tornadic categories (Thompson et al., 2002; Thompson et al., 2003). Figure 9 shows the effects of smoke on these two variables. For CAPE, although the outbreak on 4 May 2003 shows a very large increase in CAPE due to smoke, the simulation without fires has mean CAPE of ~1500 J/kg which is high enough to support the formation of supercells in the model (not shown). On the other hand, for the 27 April 2011 outbreak there is only a medium effect size showing a decrease in CAPE due to smoke. But again both simulations show mean CAPE of over 2000 J/kg, thus this difference is not expected to impact supercell formation. On the other hand, all cases show a negligible effect of smoke on 6km shear, which is different to the effects mentioned earlier for 1km shear. This indicates that changes in wind due to smoke are mostly located in the lower layers. Figure 9 also

shows Convective Inhibition (CIN), which is also a parameter used to assess the formation of supercells, indicating a small to negligible effect of smoke on this parameter. Although the smoke produces stronger CIN (i.e, more negative) for the 4 May 2003 outbreak, supercells are still generated in regions of close to zero CIN for the simulation including smoke emissions.

Why is there large variability in the smoke effects on environmental conditions although all outbreaks studied consistently show smoke presence? Figure 7 shows cloud droplet number concentrations (NDROP, middle panels) and cloud fraction (bottom panels) that can help answer this question. For instance, 4 May 2003 and 5 May 2007 show similar patterns of smoke (mostly contained in the boundary layer) and similar cloud fractions (ranging from 0.3 to 0.7 in the 0.25-1.25 km layer). However, for 4 May 2003 the impacts of smoke on NDROP in the 0.25-1.25 km layer are large (2-3 fold increase on average), while they are small for the 5 May 2007 outbreak (50-67 % increase on average), which coincides with a large and negligible effect on environmental parameters for the 4 May 2003 and 5 May 2007 outbreaks, respectively. One of the mechanisms that generate conditions where tornado formation is more likely is the optical thickening of low-level clouds through the activation of additional cloud droplets by the smoke (Saide et al., 2015b). Thus, if this additional increase in NDROP is not substantial, it is expected that environmental conditions would not change through this mechanism. 27 April 2011, which is the other outbreak with strong smoke effects, also shows a factor of 2-3 increase on average NDROP for vertical layers with cloud fractions over 0.2. Also, this outbreak presents a thick layer of smoke on top of the clouds that is expected to exacerbate the smoke effects by enhancing the capping inversion through soot absorption (Saide et al., 2015b), which in the WRF-AAM configuration is included through the SSA of the mixture. The rest of the outbreaks

either did not present cloud fractions large enough nor sufficiently large changes to the cloud droplet number concentration to produce regional effects on the environmental conditions.

Now, why does cloud droplet concentration increase due to smoke show large variability between outbreaks? Considering only the layers with cloud fractions higher than 0.2, the outbreaks with the largest NDROP increases (4 May 2003 and 27 April 2011) are those with the largest increases in aerosol number concentrations due to smoke (Figure 7). For instance, in the 250-750m layer there is a 3-6 fold increase (on average) on aerosol number concentration for the outbreaks with larger NDROP changes versus a ~2 fold increase for the rest of the outbreaks, while for the 0.75-1.25 km layer the increases are 7-9 fold versus 3-4 fold. Thus, larger aerosol number concentrations due to smoke in the cloudy layers can contribute to intensification of the outbreaks (i.e., lower LCL, larger 1km shear and SRH), but it also depends on the overlying background conditions. For instance, the 5 May 2007 outbreak presents larger aerosol number concentrations at the cloud level compared to the 27 April 2011, but since the simulation without fires shows very low aerosol number concentrations for 27 April 2011 the smoke effects are amplified in this event. The vertical location of the smoke and its ability to reach the cloud layer is also crucial, as for instance, the 28 April 2014 outbreak shows 5-6 fold enhancements in aerosol number concentration due to smoke above the cloud layer but was not mixed downward to provide large enhancements in NDROP. Other conditions affecting aerosol activation including temperature and vertical wind velocities (Thompson and Eidhammer, 2014) can change from outbreak to outbreak and could also play a role on the differences found.

3.4. Sensitivity simulations

We performed additional simulations to assess the effects of aerosol absorption and of changing the initial smoke emissions. In the case of absorption, we modified the WRF-AAM code to use single-scattering albedo (SSA) of a marine-type aerosol which absorbs radiation very weakly (SSA of 0.99 at 70% relative humidity, versus 0.95 SSA of the rural type aerosol used in the base simulations). The effect of absorption is then obtained by comparing simulations with smoke emissions using the base configuration and the configuration just described. The other set of sensitivity simulations performed used the FINN (Wiedinmyer et al., 2011) biomass burning emissions as initial estimates and followed the same emission inversion scheme. All these simulations were performed for three tornado outbreaks: 4 May 2003, 5 May 2007 and 15 April 2011. These outbreaks were chosen because they show a range of vertical smoke distributions (mostly in the boundary layer and in the lower troposphere) and smoke effects (from large to negligible effect size).

Figure 10 (top row) shows the effects of smoke on tornado parameters due to absorption. The effect of absorption can vary from negligible to medium effect size depending on the outbreak and the variable. The outbreak on 15 April 2011 presents a thick aerosol layer on top of the shallow clouds going up to 4-5 km, while the smoke layer is mostly at cloud level or below on the other two outbreaks (Figure 11, top-left panels). Previous studies have found that the location of the smoke (or absorbing aerosol) with respect to clouds can be critical for the resulting effects, with above cloud aerosol tending to increase cloudiness by enhancing the capping inversion, while in-cloud aerosol can have the ability of burn-off clouds (Feingold et al., 2005; Johnson et al., 2004). As seen in Figure 10, absorption makes LCL height shallower for the outbreak on 15 April 2011 while deeper for the other two. This is consistent with difference in the location of smoke between simulations, as for 15 April 2011 cloud fraction tends to increase when the

smoke is absorbing while it is reduced for the other two outbreaks (Figure 11, bottom-left panels). Note that for 5 May 2007 the overall effect of smoke on LCL is negligible (Figure 9, top-left panel), thus absorption is counteracting the microphysical effects resulting in no apparent effects. On the other hand, absorption tends to have a negligible effect or increase low-level wind shear and SRH for all outbreaks. The increases are likely due to stabilization of the boundary layer by aerosols on top of it. This is expected for the 15 April 2011 case due to the thick smoke layer on top, and also occurs for the 4 May 2003 probably because this outbreak has the largest smoke concentrations and the higher values are at the PBL height (Figure 7 and 8), so some of this smoke is likely sitting right on top of the PBL generating these effects.

The smoke effects when using a different set of initial smoke emissions are shown on Figure 10 center-row panels and the vertical profiles can be found on Figure 11 right panels. The sensitivity simulations are performed to assess smoke effects under different smoke loads. By comparing Figure 11 and Figure 7 it can be seen that the resulting aerosol number concentration distributions differ, with 5 May 2007 outbreak showing larger concentration enhancements due to smoke in the sensitivity simulations and the 4 May 2003 and 15 April 2011 outbreaks showing lower enhancements. The changes in smoke can have a variety of effects. For the 5 May 2007 and 15 April 2011 outbreaks the smoke effects remain similar in the sensitivity simulations (Figure 10) compared to the base-line simulations (Figure 9), i.e. negligible smoke effects for the 5 May 2007 outbreak and small effect size for the 15 April 2011. On the other hand, smoke effects change drastically for the 4 May 2003 outbreak, going from medium-large effect size for the base-line simulation (Figure 9) to small effect size on the sensitivity simulation (Figure 10). This is likely explained due to the lower aerosol loads in the sensitivity simulation which does not generate the cloud fraction enhancement shown in the base-line case (Figure 11 vs. 7).

400 However, although there are differences in the magnitude of the smoke effects, the direction of
401 the change remains the same, i.e., smoke generates an increased likelihood of tornado formation
402 and intensity for both cases.

403

404 3.5. WRF-AAM vs WRF-Chem

405 In this section we compare WRF-AAM and WRF-Chem in terms of the AOD loads and smoke
406 effects.

407 The constrained emissions are influenced by the ability of the simplified aerosol species in the
408 AAM configuration to represent AOD. Figure 6 (top panels) shows a comparison between WRF-
409 AAM and WRF-Chem AOD for one of the outbreaks studied (27 April 2011). The similarity
410 between both simulations is remarkable given the differences in the aerosol model (a full
411 chemistry sectional scheme with 8 size bins versus two aerosol species), the optical properties
412 parameterization (a Mie code including a core-shell treatment versus a table look-up approach)
413 and the cloud physics parameterizations (Morrison (Yang et al., 2011 and references therein)
414 versus TE2014 microphysics). Some of the differences between the simulations are due to the
415 way each treats the hygroscopic growth of smoke. In the case of WRF-Chem configured with
416 MOSAIC, aerosol hygroscopic growth is done through the electrolytes in the aerosol mixture,
417 and as organic carbon and black carbon are not considered as electrolytes in this model
418 configuration, there is little hygroscopic growth for smoke. For the AAM configuration the
419 opposite happens, as organic carbon emissions are lumped into the hygroscopic aerosol
420 (hygroscopicity parameter equals to 0.4) and thus undergo significant water uptake. There are
421 large differences in the northwest of the Gulf of Mexico between WRF-AAM and WRF-Chem

(Figure 6), which are due to the differences in hygroscopic growth as some model layers show large values of relative humidity (RH) in this region at this time. The localized spikes in the WRF-AAM AOD that are not seen in the WRF-Chem AOD are also due to hygroscopic growth. Thus, we expect to obtain slightly lower emission correction factors when performing the inversion with the AAM than with WRF-Chem due to the larger AOD obtained because of the hygroscopic growth of smoke.

As mentioned previously, non-negligible smoke effects are found for the 27 April 2011 outbreak when using the AAM configuration. Saide et al. (2015b), using WRF-Chem, reported 100-200 m lower LCL, ~2 m/s higher low-level wind shear and ~50 m^2/s^2 higher SRH as a result of smoke interactions with clouds and radiation, which is in the same direction and of similar values to what is found with WRF-AAM for this event (Figure 9). This agreement is again noteworthy given the complex aerosol-cloud-radiation interactions that occur in this system and the way they are parameterized differently in each model configuration (e.g., aerosol optical properties, aerosol size distribution, cloud microphysics, aerosol activation, etc.).

We performed WRF-Chem simulations for the three outbreaks studied in the sensitivity simulations (Section 3.4) to further assess similarities and differences with respect to the WRF-AAM configuration. Figures 7 and 12 (top panels) show that aerosol number concentrations for simulations with and without fire emissions are consistent within the two systems. Note that the WRF-Chem concentrations are shown only for the accumulation mode and thus aerosol number concentrations are much lower compared to WRF-AAM. Although in WRF-Chem total aerosol number is dominated by ultra-fine particles from new particle formation, these particles tend to contribute less to CCN than accumulation mode particles and thus cloud droplet numbers are

444 higher in simulations with smoke (Figure 12, center-row panels), which is consistent with WRF-
445 AAM simulations.

446 As seen in Figure 10 (bottom panels), smoke intensifies tornado parameters for all cases when
447 using WRF-Chem with effect size on the small to medium range. This is generally consistent
448 with the WRF-AAM simulations, as with this system the 4 May 2003 and 15 April 2011
449 outbreaks show intensification with small to large effect size, while 5 May 2007 shows
450 negligible effects (Figure 9 top panels). There could be multiple reasons for these discrepancies.
451 For instance, for the 4 May 2003 outbreak the enhancement in cloud droplet number
452 concentration due to smoke for WRF-AAM (Figure 7) is larger than for WRF-Chem (Figure 12)
453 which contributes to a larger effect size in tornado parameters for WRF-AAM for this outbreak.
454 The higher cloud droplet number concentration in WRF-AAM could be due to the differences
455 between the aerosol activation parameterizations in WRF-Chem and WRF-AAM as droplet
456 nucleation could get saturated at different aerosol loadings. Aerosol optical properties could also
457 be producing some of these differences, as the smoke is more absorbing on WRF-Chem (SSA of
458 0.93-0.94 on the region of the 4 May 2003 outbreak) than on WRF-AAM (SSA over 0.96 for RH
459 over 80%), thus the burn-off of clouds due to absorption found in section 3.4 for the 4 May 2003
460 outbreak could be occurring more efficiently in WRF-Chem and thus preventing the large
461 enhancement in cloud fraction seen in WRF-AAM. For the 5 May 2007 outbreak the aerosol
462 concentrations are maximum at the surface, which generates a different response in WRF-AAM
463 and WRF-Chem, with WRF-Chem increasing cloud fractions due to smoke at the lower levels
464 (below 750m) and thus intensifying the tornado parameters where in WRF-AAM only negligible
465 changes are found.

466 **4. Conclusions**

In this study we used the WRF modeling system configured with an aerosol-aware microphysics (AAM) parameterization to study impacts of smoke from Central America on multiple tornado outbreaks in the US happening during the fire season. To do so, we included emission processes into the WRF-AAM by using WRF-Chem routines that add primary aerosol emissions to the model. Also, we constrained biomass burning emissions for each outbreak studied using satellite-derived AOD and an inverse modeling algorithm. We found a general underestimation of the prior emissions but with large spatial and temporal variations. This is important as studies not using an observational constraint are likely to underestimate the smoke effects, and this cannot be fixed by just applying a global correction factor to emissions.

Using the WRF aerosol-aware-microphysics configuration, we found smoke present in the boundary layer of all outbreaks studied with some cases presenting a thick layer of smoke aloft. Across the various cases studied, we also found a large spread of the smoke effects on environmental conditions, going from negligible impacts to intensifications due to smoke (i.e., a reduction of LCL and increase in low level wind shear and SRH) which are in the range of differences found in the sounding climatology within adjacent supercell classes (Thompson et al., 2003). Smoke effects on environmental conditions were considerable when there was a distinct layer of low level clouds (cloud fraction >0.2) and the smoke largely increased aerosol number concentration over background values (3-9 fold), producing large cloud droplet concentration increases (2-3 fold). We found that the presence of a thick layer of smoke above the low-level clouds can contribute to the intensifications of tornado parameters. However, when this layer is not present and smoke concentration at cloud level is large, aerosol absorption can produce cloud-burn off which can deepen the LCL heights, counteracting the microphysical effects. Sensitivity simulations also showed that when changing smoke emissions the smoke

effects on tornado parameters were consistent but the magnitudes could vary with the emissions amount.

In this study we only analyzed the effects of biomass burning smoke on environmental conditions that lead to a higher likelihood of tornado formation and intensity. Other studies have proposed alternative mechanisms such as convection invigoration to link smoke with tornadoes (Wang et al., 2009), or suggested that tornado occurrence have a weekly cycle due to anthropogenic activities (Rosenfeld and Bell, 2011). Recent evidence has shown that fires also present a weekly cycle (Earl et al., 2015). Given our finding that smoke was present for all outbreaks studied, and that can be a major contributor to aerosol number concentrations in all the cases, the role of fires in these other mechanisms needs to be included in future work studying tornadoes during the fire season. Also, given that the Gulf of Mexico is a common source of moisture for severe thunderstorms (Brooks et al., 2003), we expect smoke to be transported along with moisture during the burning season, thus future work should assess the effects of smoke for severe weather other than tornadoes (e.g., large hail and damaging winds).

Finally, we also compared WRF configured with aerosol-aware-microphysics to WRF-Chem. Although these model configurations use different parameterizations of aerosol optical properties, aerosol size, cloud microphysics and cloud droplet nucleation, we found their results are generally consistent. In particular, they show comparable AODs over the region affected with smoke, similar smoke transport patterns to the outbreak region and consistent smoke effects on environmental conditions which can lead to intensification of the outbreak. Thus, the aerosol-cloud-radiation interactions included in WRF-AAM are generally in agreement with more complex models and given the current restrictions on computing power dedicated to these interactions they represent a good choice for the moment. This is encouraging as the AAM is

planned to become one of National Centers for Environmental Prediction (NCEP) operational configurations (Rapid Refresh and High-Resolution Rapid Refresh forecasts). The method to constrain emissions coupled to the WRF-AAM is also computationally efficient as it only requires two simulations (no adjoint, no ensembles), thus it could be implemented in near-real time applications to constrain highly uncertain emissions such as those from fires and wind-blown dust.

Acknowledgments

The National Center for Atmospheric Research is supported by the National Science Foundation. Contact P.E. Saide (saide@ucar.edu) for data and code requests. This work was carried out with the aid of NASA grant NNXAF95G. A. M. da Silva is funded by NASA's Modeling and Application Program. We acknowledge use of MOZART-4 global model output available at http://www.acom.ucar.edu/wrf-chem/mozart.shtml. CALIPSO data were obtained from the NASA Langley Research Center Atmospheric Science Data Center (https://earthdata.nasa.gov/). The views, opinions, and findings contained in this report are those of the author(s) and should not be construed as an official National Oceanic and Atmospheric Administration or U.S. Government position, policy, or decision.

References

Abdul-Razzak, H. and Ghan, S. J.: A parameterization of aerosol activation 3. Sectional representation, J. Geophys. Res., 107, 4026, 2002.

Andreae, M. O. and Rosenfeld, D.: Aerosol–cloud–precipitation interactions. Part 1. The nature and sources of cloud-active aerosols, Earth-Science Reviews, 89, 13-41, 2008.

Barlage, M., Chen, F., Tewari, M., Ikeda, K., Gochis, D., Dudhia, J., Rasmussen, R., Livneh, B., Ek, M., and Mitchell, K.: Noah land surface model modifications to improve snowpack prediction in the Colorado Rocky Mountains, Journal of Geophysical Research: Atmospheres, 115, D22101, 2010.

Barrett, B. S. and Gensini, V. A.: Variability of central United States April–May tornado day likelihood by phase of the Madden-Julian Oscillation, Geophysical Research Letters, 40, 2790-2795, 2013.

Blunden, J. and Arndt, D. S.: State of the Climate in 2011, Bulletin of the American Meteorological Society, 93, S1-S282, 2012.

543 Blunden, J. and Arndt, D. S.: State of the Climate in 2013, Bulletin of the American
544 Meteorological Society, 95, S1-S279, 2014.

545 Blunden, J. and Arndt, D. S.: State of the Climate in 2014, Bulletin of the American
546 Meteorological Society, 96, ES1-ES32, 2015.

547 Bond, T. C., Streets, D. G., Yarber, K. F., Nelson, S. M., Woo, J.-H., and Klimont, Z.: A
548 technology-based global inventory of black and organic carbon emissions from combustion,
549 Journal of Geophysical Research: Atmospheres, 109, D14203, 2004.

550 Boucher, O., Randall, D., Artaxo, P., Bretherton, C., Feingold, G., Forster, P., Kerminen, V.-M.,
551 Kondo, Y., Liao, H., Lohmann, U., Rasch, P., Satheesh, S. K., Sherwood, S., Stevens, B., and
552 Zhang, X. Y.: Clouds and Aerosols. In: Climate Change 2013: The Physical Science Basis.
553 Contribution of Working Group I to the Fifth Assessment Report of the Intergovernmental 25
554 Panel on Climate Change, edited by: Stocker, T. F., Qin, D., Plattner, G.-K., Tignor, M., Allen,
555 S. K., Boschung, J., Nauels, A., Xia, Y., Bex, V., and Midgley, P. M, Cambridge University
556 Press, Cambridge, United Kingdom and New York, NY, USA, 2013.

557 Brooks, H. E.: Severe thunderstorms and climate change, Atmospheric Research, 123, 129-138,
558 2013.

559 Brooks, H. E. and Doswell, C. A.: Deaths in the 3 May 1999 Oklahoma City Tornado from a
560 Historical Perspective, Weather and Forecasting, 17, 354-361, 2002.

561 Brooks, H. E., Lee, J. W., and Craven, J. P.: The spatial distribution of severe thunderstorm and
562 tornado environments from global reanalysis data, Atmospheric Research, 67–68, 73-94, 2003.

563 Darmenov, A. and da Silva, A. M.: The Quick Fire Emissions Dataset (QFED) - Documentation
564 of versions 2.1, 2.2 and 2.4, NASA/TM–2015–104606, Vol. 38., (
565 http://gmao.gsfc.nasa.gov/pubs/tm/), 183 pp, 2015.

566 Diffenbaugh, N. S., Scherer, M., and Trapp, R. J.: Robust increases in severe thunderstorm
567 environments in response to greenhouse forcing, Proceedings of the National Academy of
568 Sciences, 110, 16361-16366, 2013.

569 Earl, N., Simmonds, I., and Tapper, N.: Weekly cycles of global fires—Associations with
570 religion, wealth and culture, and insights into anthropogenic influences on global climate,
571 Geophysical Research Letters, 42, 2015GL066383, 2015.

572 Eidhammer, T., Barth, M. C., Petters, M. D., Wiedinmyer, C., and Prenni, A. J.: Aerosol
573 microphysical impact on summertime convective precipitation in the Rocky Mountain region,
574 Journal of Geophysical Research: Atmospheres, 2014JD021883, 2014.

575 Emmons, L. K., Walters, S., Hess, P. G., Lamarque, J. F., Pfister, G. G., Fillmore, D., Granier,
576 C., Guenther, A., Kinnison, D., Laepple, T., Orlando, J., Tie, X., Tyndall, G., Wiedinmyer, C.,
577 Baughcum, S. L., and Kloster, S.: Description and evaluation of the Model for Ozone and
578 Related chemical Tracers, version 4 (MOZART-4), Geosci. Model Dev., 3, 43-67, 2010.

579 Feingold, G., Jiang, H., and Harrington, J. Y.: On smoke suppression of clouds in Amazonia,
580 Geophysical research letters, 32, L02804, 2005.

581 Freitas, S. R., Longo, K. M., Alonso, M. F., Pirre, M., Marecal, V., Grell, G., Stockler, R., Mello,
582 R. F., and Sánchez Gácita, M.: PREP-CHEM-SRC – 1.0: a preprocessor of trace gas and aerosol
583 emission fields for regional and global atmospheric chemistry models, Geosci. Model Dev., 4,
584 419-433, 2011.

585 GMAO: http://gmao.gsfc.nasa.gov/forecasts, 2014.

586 Gong, S., Barrie, L., and Blanchet, J.-P.: Modeling sea-salt aerosols in the atmosphere 1. Model
587 development, Journal of Geophysical Research, 102, 3805-3818, 1997.

588 Grell, G., Freitas, S. R., Stuefer, M., and Fast, J.: Inclusion of biomass burning in WRF-Chem:
589 impact of wildfires on weather forecasts, Atmos. Chem. Phys., 11, 5289-5303, 2011.

590 Grell, G. A. and Freitas, S. R.: A scale and aerosol aware stochastic convective parameterization
591 for weather and air quality modeling, Atmos. Chem. Phys. Discuss., 13, 23845-23893, 2013.

592 Hamill, T. M., Schneider, R. S., Brooks, H. E., Forbes, G. S., Bluestein, H. B., Steinberg, M.,
593 Meléndez, D., and Dole, R. M.: The May 2003 Extended Tornado Outbreak, Bulletin of the
594 American Meteorological Society, 86, 531-542, 2005.

595 Holben, B., Tanré, D., Smirnov, A., Eck, T., Slutsker, I., Abuhassan, N., Newcomb, W., Schafer,
596 J., Chatenet, B., and Lavenu, F.: An emerging ground-based aerosol climatology: Aerosol optical
597 depth from AERONET, Journal of Geophysical Research, 106, 12067-12012,12097, 2001.

598 Iacono, M. J., Delamere, J. S., Mlawer, E. J., Shephard, M. W., Clough, S. A., and Collins, W.
599 D.: Radiative forcing by long-lived greenhouse gases: Calculations with the AER radiative
600 transfer models, Journal of Geophysical Research: Atmospheres, 113, D13103, 2008.

601 Iacono, M. J., Mlawer, E. J., Clough, S. A., and Morcrette, J.-J.: Impact of an improved
602 longwave radiation model, RRTM, on the energy budget and thermodynamic properties of the
603 NCAR community climate model, CCM3, Journal of Geophysical Research: Atmospheres, 105,
604 14873-14890, 2000.

605 Jacobson, M. Z.: Effects of biomass burning on climate, accounting for heat and moisture fluxes,
606 black and brown carbon, and cloud absorption effects, Journal of Geophysical Research:
607 Atmospheres, 2014JD021861, 2014.

608 Janjić, Z. I.: Nonsingular implementation of the Mellor–Yamada level 2.5 scheme in the NCEP
609 Meso model, NCEP office note, 437, 61, 2002.

610 Johnson, B. T., Shine, K. P., and Forster, P. M.: The semi-direct aerosol effect: Impact of
611 absorbing aerosols on marine stratocumulus, Quarterly Journal of the Royal Meteorological
612 Society, 130, 1407-1422, 2004.

Kaiser, J. W., Heil, A., Andreae, M. O., Benedetti, A., Chubarova, N., Jones, L., Morcrette, J. J., Razinger, M., Schultz, M. G., Suttie, M., and van der Werf, G. R.: Biomass burning emissions estimated with a global fire assimilation system based on observed fire radiative power, Biogeosciences, 9, 527-554, 2012.

Knupp, K. R., Murphy, T. A., Coleman, T. A., Wade, R. A., Mullins, S. A., Schultz, C. J., Schultz, E. V., Carey, L., Sherrer, A., McCaul, E. W., Carcione, B., Latimer, S., Kula, A., Laws, K., Marsh, P. T., and Klockow, K.: Meteorological Overview of the Devastating 27 April 2011 Tornado Outbreak, Bulletin of the American Meteorological Society, 2013.

Kolusu, S. R., Marsham, J. H., Mulcahy, J., Johnson, B., Dunning, C., Bush, M., and Spracklen, D. V.: Impacts of Amazonia biomass burning aerosols assessed from short-range weather forecasts, Atmos. Chem. Phys., 15, 12251-12266, 2015.

Lebo, Z. J. and Morrison, H.: A Novel Scheme for Parameterizing Aerosol Processing in Warm Clouds, Journal of the Atmospheric Sciences, 70, 3576-3598, 2013.

Levinson, D. H. and Lawrimore, J. H.: State of the Climate in 2007, Bulletin of the American Meteorological Society, 89, S1-S179, 2008.

Levinson, D. H. and Waple, A. M.: State of the Climate in 2003, Bulletin of the American Meteorological Society, 85, 881-881, 2004.

Markowski, P. M. and Richardson, Y. P.: Tornadogenesis: Our current understanding, forecasting considerations, and questions to guide future research, Atmospheric Research, 93, 3-10, 2009.

Mena-Carrasco, M., Carmichael, G. R., Campbell, J. E., Zimmerman, D., Tang, Y., Adhikary, B., D'Allura, A., Molina, L. T., Zavala, M., García, A., Flocke, F., Campos, T., Weinheimer, A. J., Shetter, R., Apel, E., Montzka, D. D., Knapp, D. J., and Zheng, W.: Assessing the regional impacts of Mexico City emissions on air quality and chemistry, Atmos. Chem. Phys., 9, 3731-3743, 2009.

NCEP: NCEP FNL Operational Model Global Tropospheric Analyses, continuing from July 1999. Research Data Archive at the National Center for Atmospheric Research, Computational and Information Systems Laboratory, Boulder, CO, 2000.

Peterson, T. C. and Baringer, M. O.: State of the Climate in 2008, Bulletin of the American Meteorological Society, 90, S1-S196, 2009.

Potter, S.: Fine-Tuning Fujita: After 35 years, a new scale for rating tornadoes takes effect, Weatherwise, 60, 64-71, 2007.

Rasmussen, E. N. and Blanchard, D. O.: A Baseline Climatology of Sounding-Derived Supercell and Tornado Forecast Parameters, Weather and Forecasting, 13, 1148-1164, 1998.

Reid, J. S., Prins, E. M., Westphal, D. L., Schmidt, C. C., Richardson, K. A., Christopher, S. A., Eck, T. F., Reid, E. A., Curtis, C. A., and Hoffman, J. P.: Real-time monitoring of South

649 American smoke particle emissions and transport using a coupled remote sensing/box-model
650 approach, Geophysical Research Letters, 31, L06107, 2004.

651 Rosenfeld, D. and Bell, T. L.: Why do tornados and hailstorms rest on weekends?, Journal of
652 Geophysical Research (Atmospheres), 116, 20211, 2011.

653 Ruiz-Arias, J. A., Dudhia, J., and Gueymard, C. A.: A simple parameterization of the short-wave
654 aerosol optical properties for surface direct and diffuse irradiances assessment in a numerical
655 weather model, Geosci. Model Dev., 7, 1159-1174, 2014.

656 Saide, P. E., Carmichael, G. R., Liu, Z., Schwartz, C. S., Lin, H. C., da Silva, A. M., and Hyer,
657 E.: Aerosol optical depth assimilation for a size-resolved sectional model: impacts of
658 observationally constrained, multi-wavelength and fine mode retrievals on regional scale
659 analyses and forecasts, Atmos. Chem. Phys., 13, 10425-10444, 2013.

660 Saide, P. E., Peterson, D., da Silva, A., Anderson, B., Ziemba, L. D., Diskin, G., Sachse, G.,
661 Hair, J., Butler, C., Fenn, M., Jimenez, J. L., Campuzano-Jost, P., Perring, A. E., Schwarz, J. P.,
662 Markovic, M. Z., Russell, P., Redemann, J., Shinozuka, Y., Streets, D. G., Yan, F., Dibb, J.,
663 Yokelson, R., Toon, O. B., Hyer, E., and Carmichael, G. R.: Revealing important nocturnal and
664 day-to-day variations in fire smoke emissions through a multiplatform inversion, Geophysical
665 research letters, 2015GL063737, 2015a.

666 Saide, P. E., Spak, S. N., Pierce, R. B., Otkin, J. A., Schaack, T. K., Heidinger, A. K., da Silva,
667 A. M., Kacenelenbogen, M., Redemann, J., and Carmichael, G. R.: Central American biomass
668 burning smoke can increase tornado severity in the U.S, Geophysical research letters, 42,
669 2014GL062826, 2015b.

670 Sullivan, G. M. and Feinn, R.: Using Effect Size—or Why the P Value Is Not Enough, Journal of
671 Graduate Medical Education, 4, 279-282, 2012.

672 Thompson, G. and Eidhammer, T.: A Study of Aerosol Impacts on Clouds and Precipitation
673 Development in a Large Winter Cyclone, Journal of the atmospheric sciences, 71, 3636-3658,
674 2014.

675 Thompson, R. L., Edwards, R., and Hart, J. A.: Evaluation and interpretation of the Supercell
676 Composite and the Significant Tornado Parameters at the Storm Prediction Centre. Preprints,
677 21st Conf. on Severe Local Storms, San Antonio, TX, Amer. Meteor. Soc., J11-J14, 2002.

678 Thompson, R. L., Edwards, R., Hart, J. A., Elmore, K. L., and Markowski, P.: Close Proximity
679 Soundings within Supercell Environments Obtained from the Rapid Update Cycle, Weather and
680 Forecasting, 18, 1243-1261, 2003.

681 Wang, J., Christopher, S. A., Nair, U. S., Reid, J. S., Prins, E. M., Szykman, J., and Hand, J. L.:
682 Mesoscale modeling of Central American smoke transport to the United States: 1. “Top-down”
683 assessment of emission strength and diurnal variation impacts, Journal of Geophysical Research:
684 Atmospheres, 111, D05S17, 2006.

685 Wang, J., van den Heever, S., and Reid, J.: A conceptual model for the link between Central
686 American biomass burning aerosols and severe weather over the south central United States,
687 Environmental Research Letters, 4, 015003, 2009.

688 Wiedinmyer, C., Akagi, S. K., Yokelson, R. J., Emmons, L. K., Al-Saadi, J. A., Orlando, J. J.,
689 and Soja, A. J.: The Fire INventory from NCAR (FINN): a high resolution global model to
690 estimate the emissions from open burning, Geosci. Model Dev., 4, 625-641, 2011.

691 Wolf, M. E., Fields, P. G., Manne, G. K., Villegas, M. T. L., Bravo, V. G., Gómez, R. I.,
692 Periférico, C., Cuicuilco, C. I., and Coyoacán, D.: Developing Mexico National Emissions
693 Inventory Projections for the Future Years of 2008, 2012, and 2030, 2009.

694 Yang, Q., W. I. Gustafson, J., Fast, J. D., Wang, H., Easter, R. C., Morrison, H., Lee, Y. N.,
695 Chapman, E. G., Spak, S. N., and Mena-Carrasco, M. A.: Assessing regional scale predictions of
696 aerosols, marine stratocumulus, and their interactions during VOCALS-REx using WRF-Chem,
697 Atmospheric Chemistry and Physics, 11, 11951-11975, 2011.

698 Zaveri, R. A., Easter, R. C., Fast, J. D., and Peters, L. K.: Model for simulating aerosol
699 interactions and chemistry (MOSAIC), J. Geophys. Res, 113, D13204, 2008.

700 Zaveri, R. A. and Peters, L. K.: A new lumped structure photochemical mechanism for large-
701 scale applications, Journal of Geophysical Research, 104, 30387-30330,30415, 1999.

702 Zhang, F., Wang, J., Ichoku, C., Hyer, E. J., Yang, Z., Ge, C., Su, S., Zhang, X., Kondragunta,
703 S., and Kaiser, J. W.: Sensitivity of mesoscale modeling of smoke direct radiative effect to the
704 emission inventory: a case study in northern sub-Saharan African region, Environmental
705 Research Letters, 9, 075002, 2014.

706 Zhao, C., Liu, X., Leung, L. R., Johnson, B., McFarlane, S. A., Gustafson Jr, W. I., Fast, J. D.,
707 and Easter, R.: The spatial distribution of mineral dust and its shortwave radiative forcing over
708 North Africa: modeling sensitivities to dust emissions and aerosol size treatments, Atmos. Chem.
709 Phys., 10, 8821-8838, 2010.

Figures

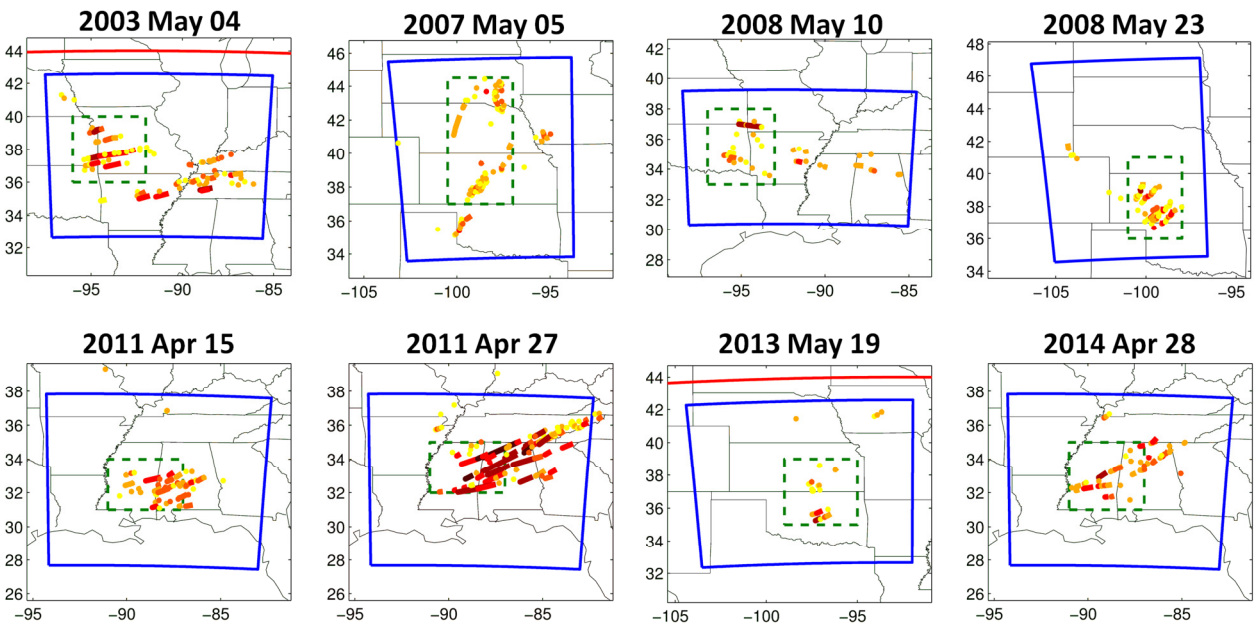

Figure 1. Tornado tracks of the outbreaks studied color-coded by Enhanced Fujita (EF) Scale (Potter, 2007), with darker colors representing higher magnitude. Blue solid lines represent the inner domain specified for each simulation. Boundaries of the outer domain are in red solid lines when included in the regions shown (see full outer domains in Figure 2). Green segmented lines show the region where statistics are computed which corresponds to the area where the earlier tornadoes occur.

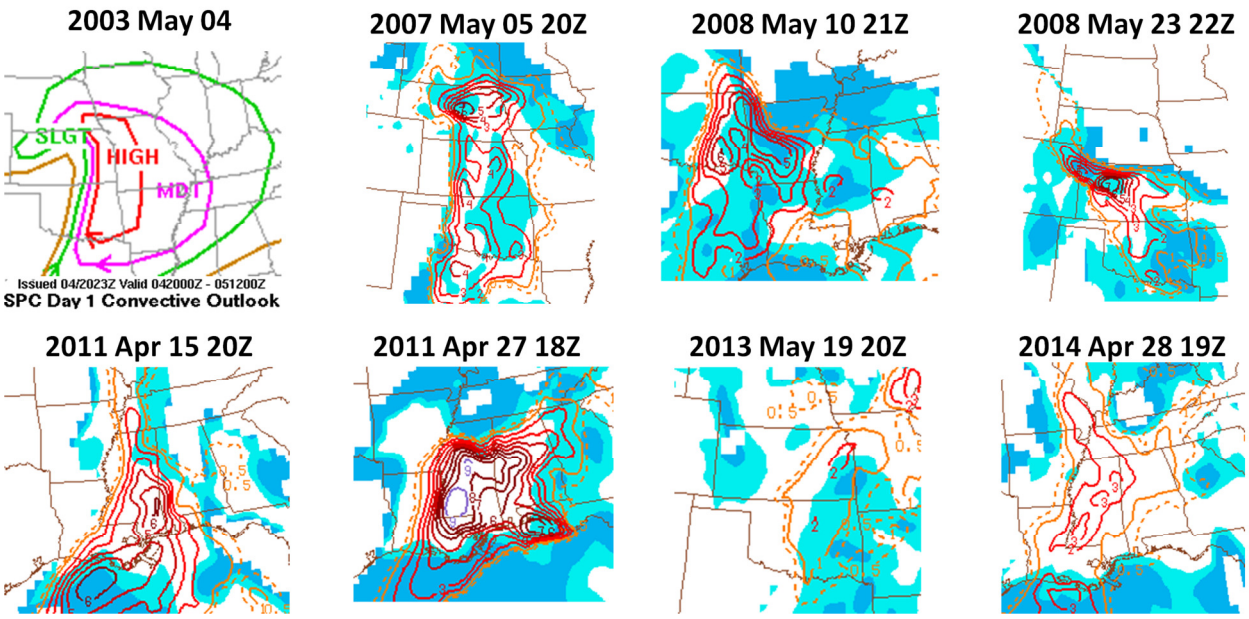

718

719 Figure 2. Environmental conditions for the outbreaks studied as provided by the SPC. While the
720 day 1 convective outlook valid at 23 UTC is shown for 2003 May 4, the fixed-layer Significant
721 Tornado Parameter (STP, in contours) and the Convective Inhibition (CIN, shaded at 25 and 100
722 J/kg) obtained from the houlrly Mesoscale Analysis are shown for the rest of the outbreaks.

723

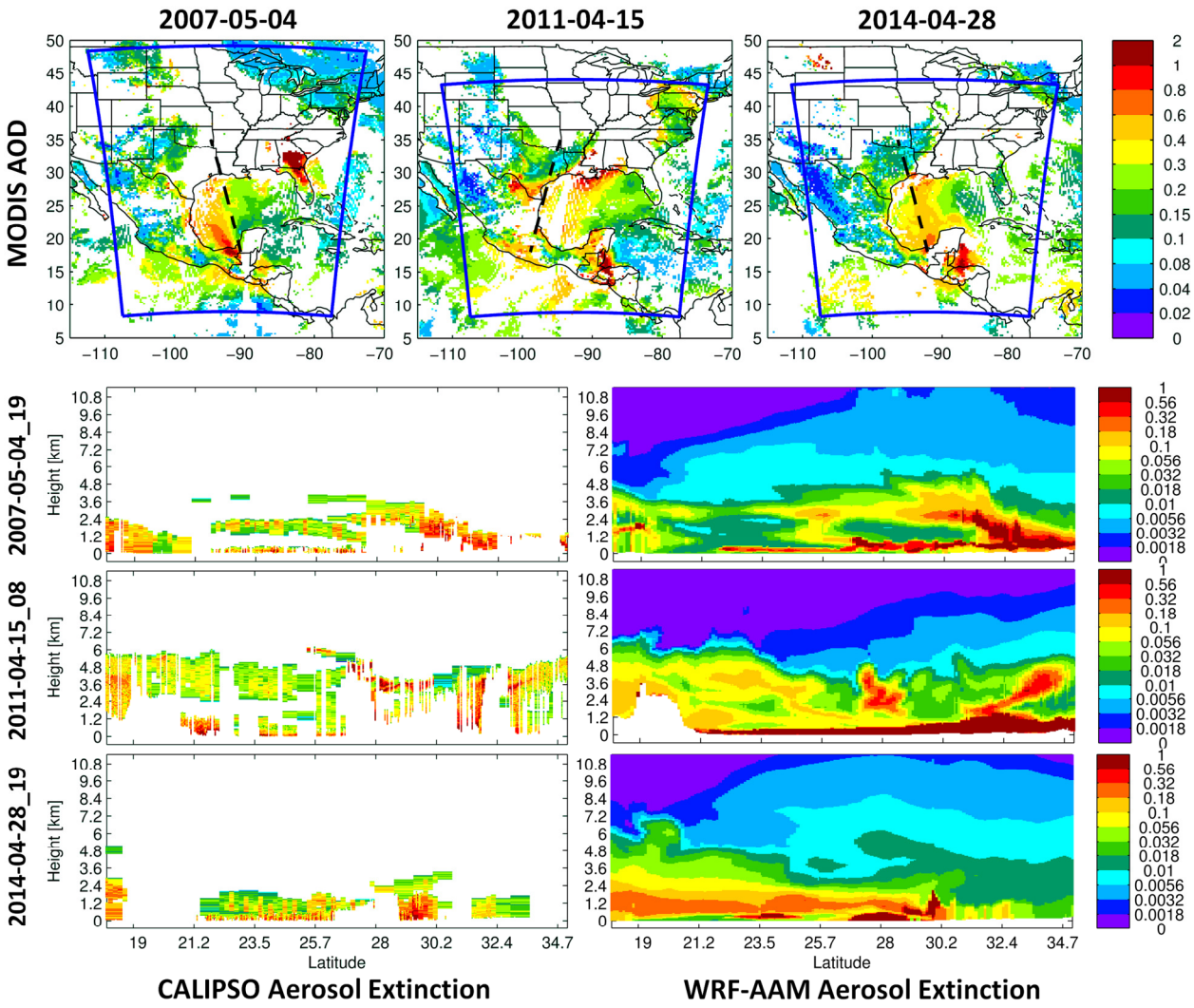

724

725 Figure 3. Top panels: Observed AOD maps on the day or the day before of three outbreaks
726 studied (5 May 2007 on the left, 15 April 2011 on the middle, and 28 April 2014 on the right) by
727 combining Terra and Aqua overpasses. The solid blue line represents the outer domains used for
728 these outbreaks. Bottom panels: Observed and modeled (Fire ON + inversion) extinction (1/km)
729 curtains. The CALIPSO tracks corresponding to these observations are shown as dashed black
730 lines on the top panels.

731

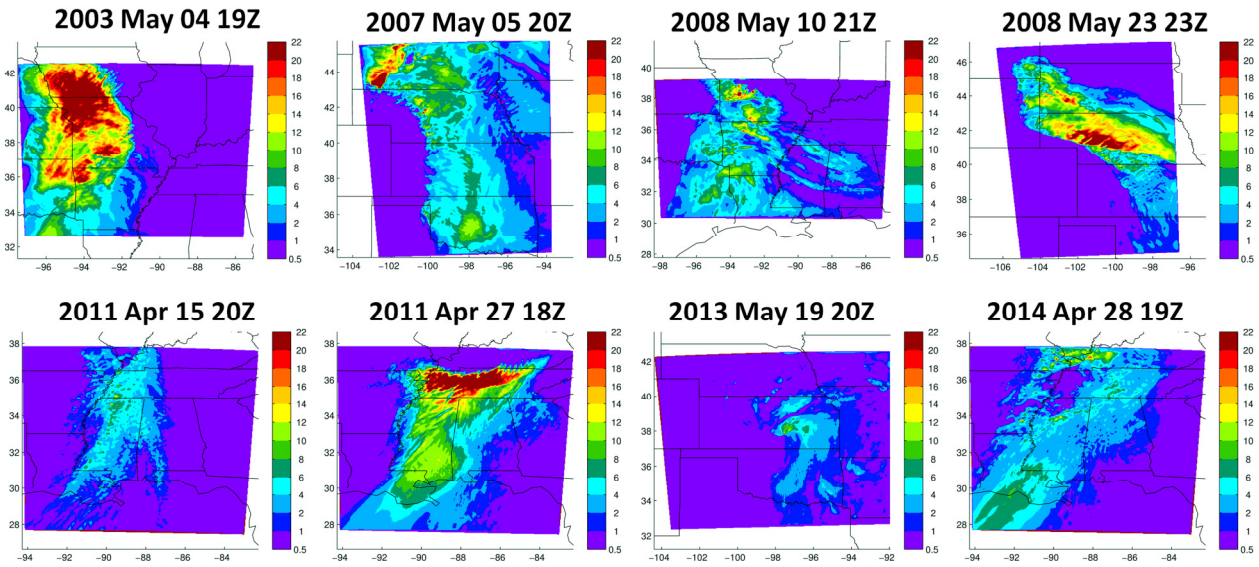

732

733 Figure 4. Significant Tornado Parameter (STP) at the beginning of each outbreak studied as

734 modeled by the WRF-AAM configuration when using the contrained fire emissions.

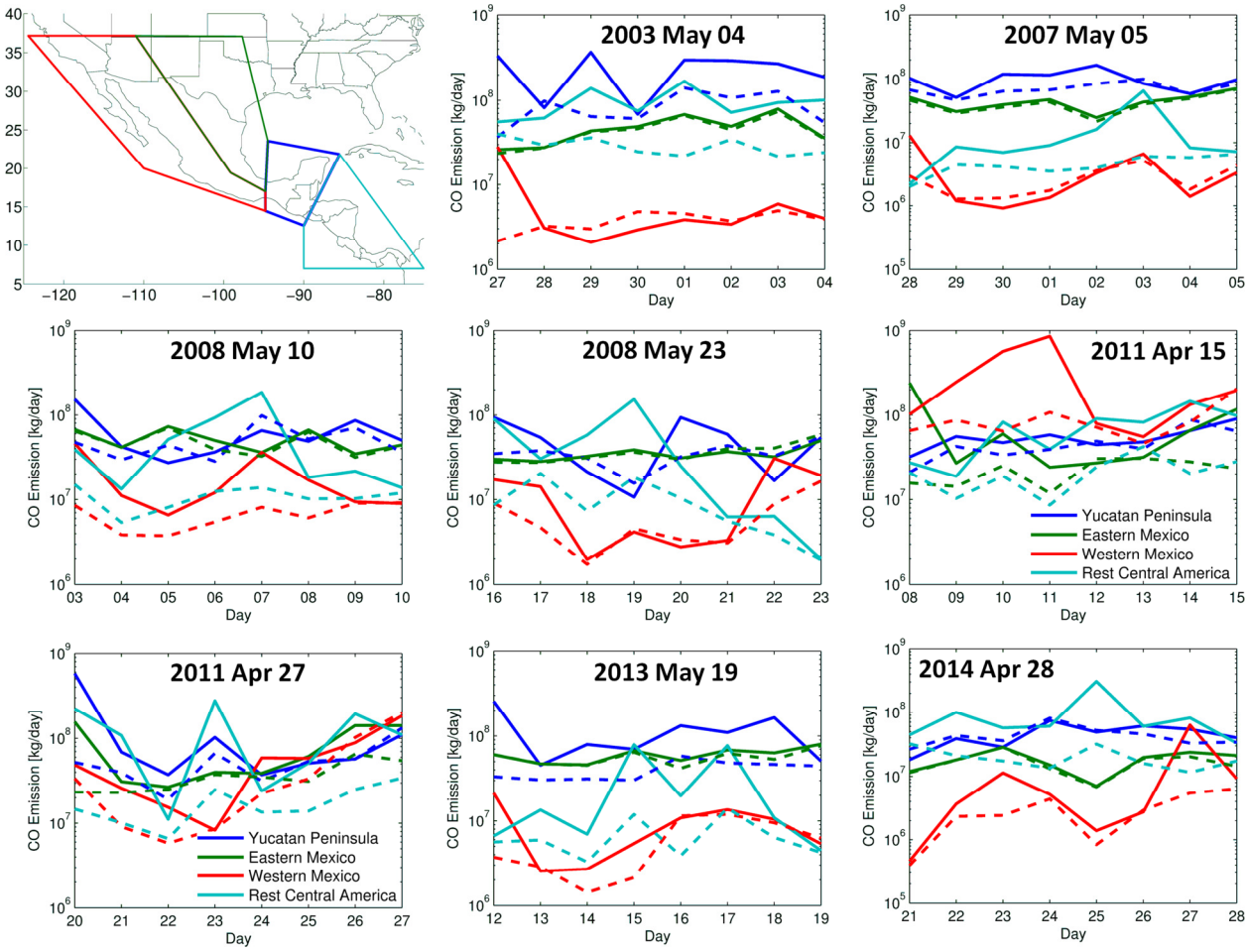

735

736 Figure 5. Top-left panel: Regions used to tag fire emissions tracers (see Section 2.3). Rest of the
737 panels: Constrained (solid lines) and first-guess (segmented lines) emissions by day on each
738 region and for each outbreak (indicated at the top of each panel).

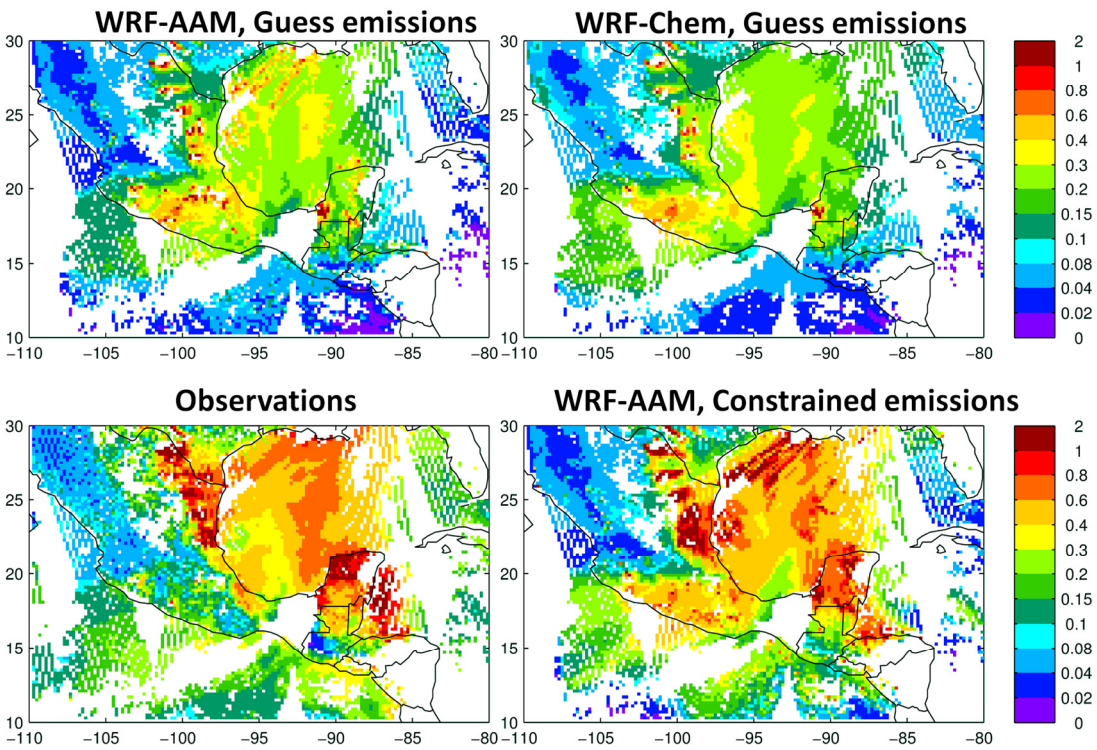

739

740 Figure 6. AOD maps for the observations and three model simulations on 27 April 2011 by
741 combining Terra and Aqua overpasses. Cloudy grid-cells are not considered when computing
742 model AOD.

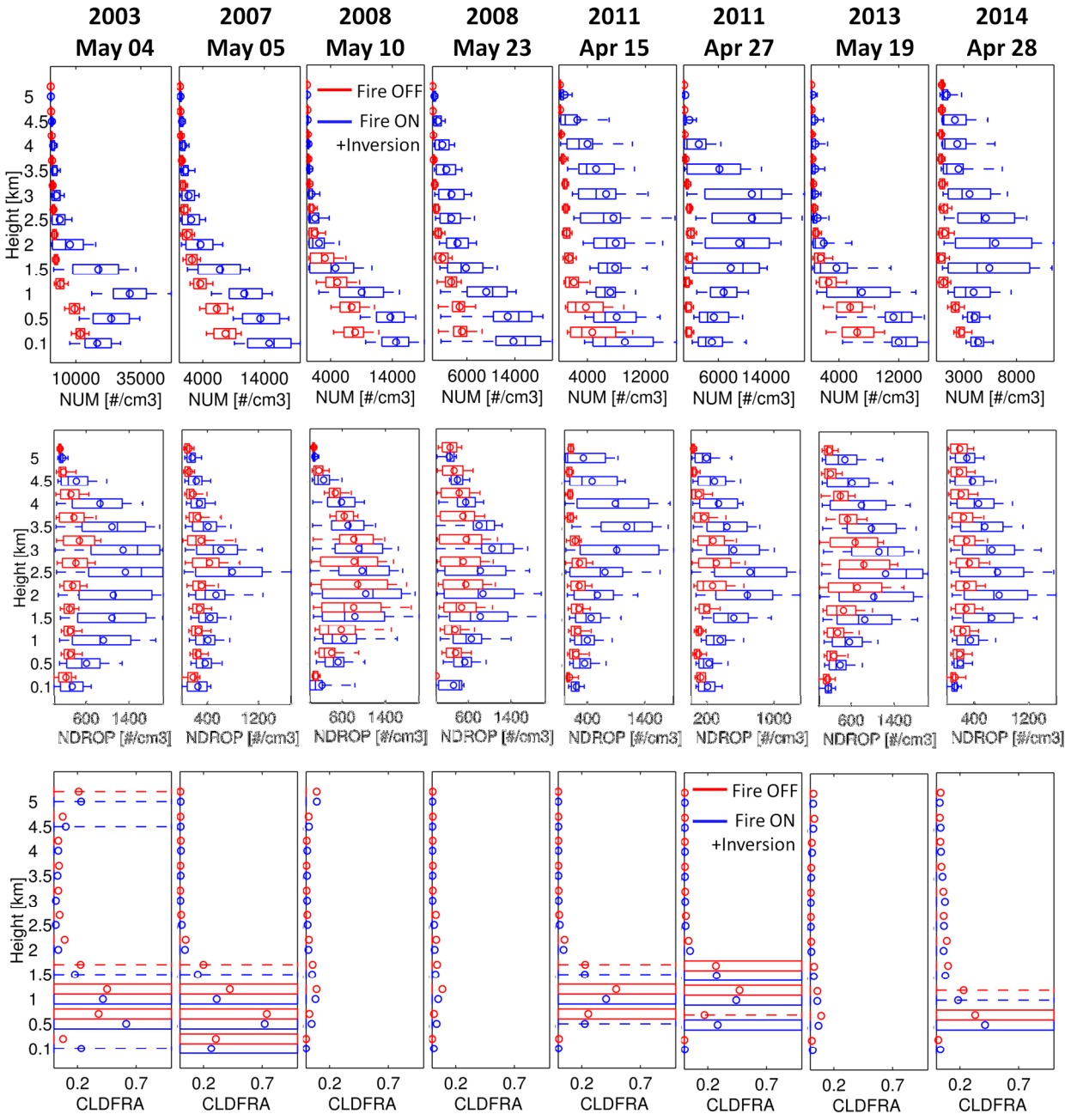

743

744 Figure 7. Vertical distributions of modeled (WRF-AAM) aerosol number concentration (NUM),
745 cloud droplet concentration (NDROP), and cloud fraction (CLDFRA) for the cases studied
746 turning on and off biomass burning emissions. The distributions are shown as box plots, with
747 center solid lines indicate the median, circles representing the mean, boxes indicating upper and
748 lower quartiles, and whiskers showing the upper and lower deciles. Statistics are computed for

749 the regions shown in Figure 1 and one hour before the outbreak starts. Note that cloud fraction is
750 either 0 or 1 in this WRF configuration, thus the boxes and whiskers either use the whole 0-1
751 interval or collapse to zero for low cloud fractions. X-axes start at a value of 0 for all panels.

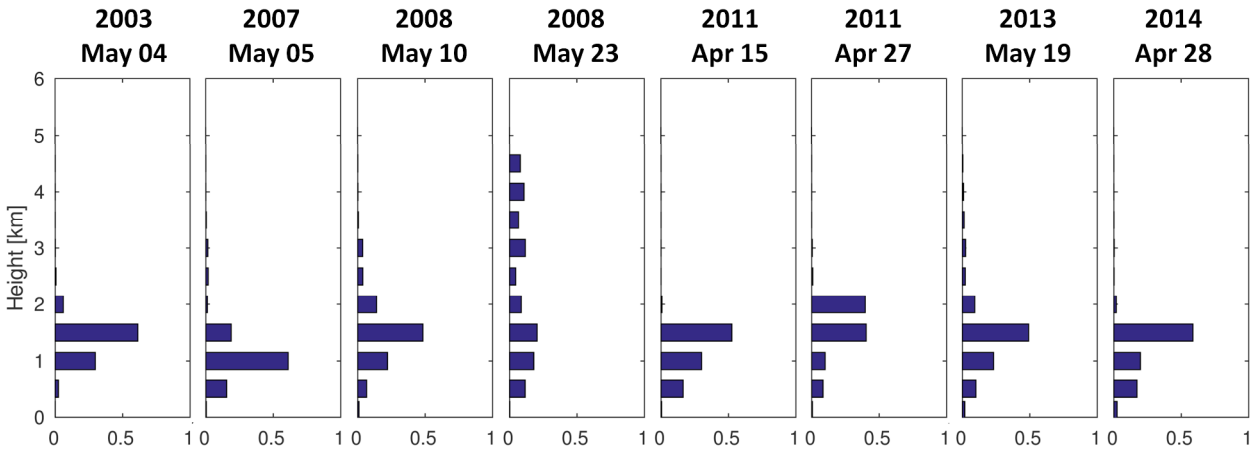

752

753 Figure 8. Normalized histograms of boundary layer height for the same regions, height
754 categories and outbreaks as in Figure 7.

755

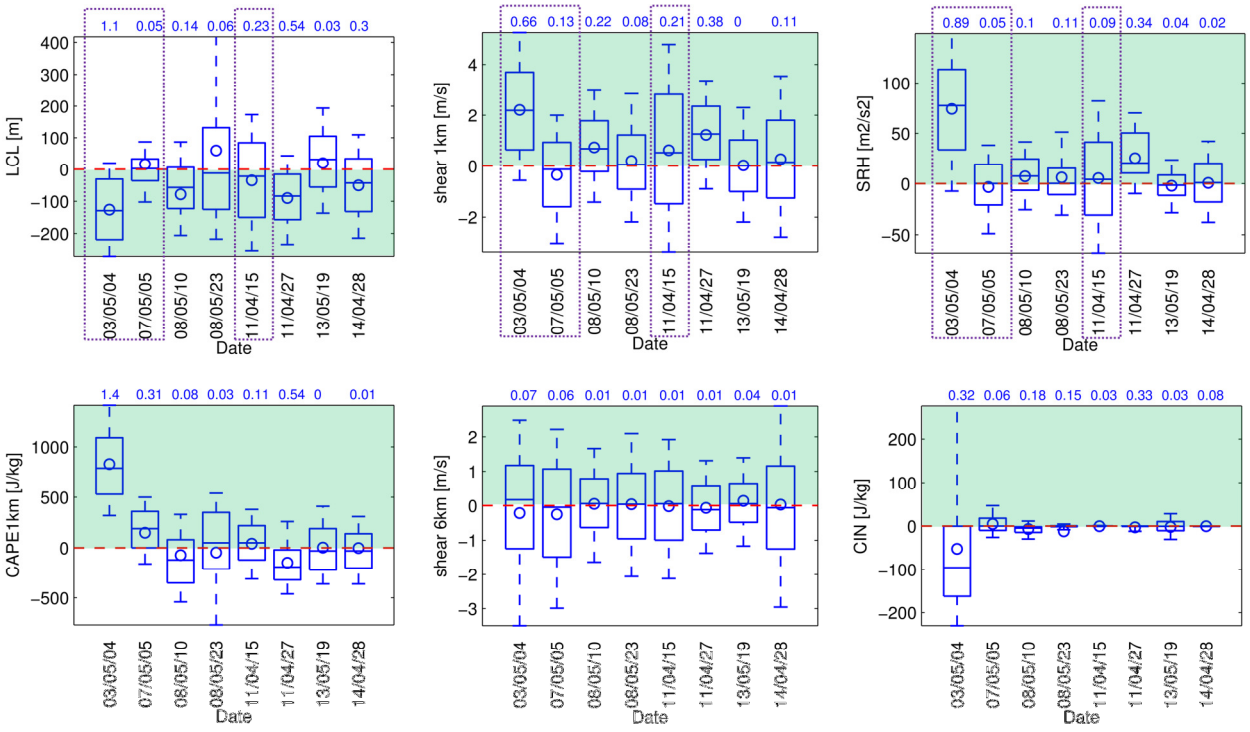

Figure 9. Statistics (as in Figure 7) of the differences between WRF-AAM simulations with and without fire emissions. The standardized difference (effect size) between both simulations is shown on top of each panel. The dashed red lines indicate the zero difference line, while the green area denotes the region where the smoke increases the likelihood of tornado occurrence and intensity (decrease in LCL, increase in 1km shear and SRH) and a higher chance of convection (increased CAPE, 6km shear and CIN). The dotted purple rectangles highlight the sensitivity cases and variables studied in the next figures. Note that CIN is a negative quantity. Dates are in YY/MM/DD format.

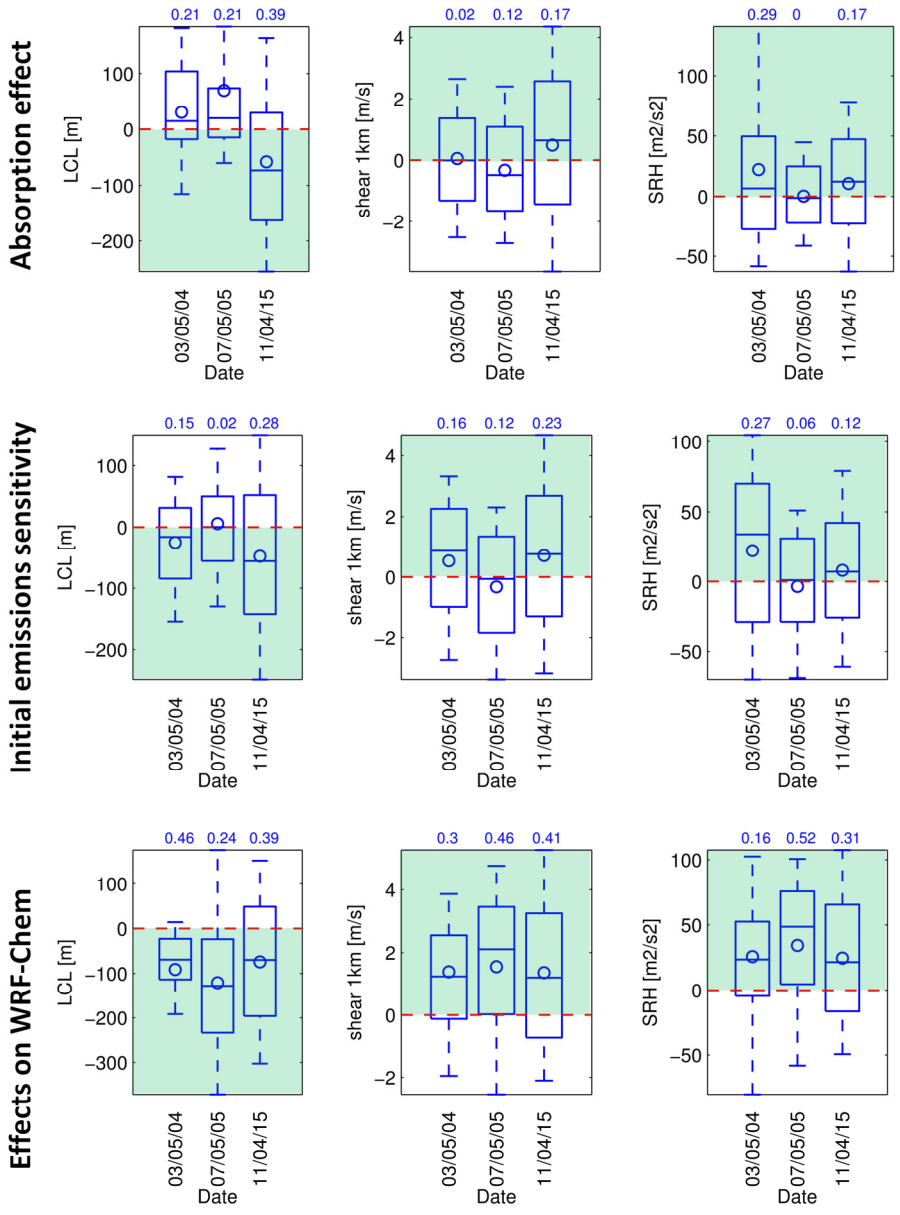

767

768 Figure 10. As Figure 9 but for the sensitivity cases and WRF-Chem simulations. Note that
769 sensitivity runs for testing the effect of absortion compare two simulations with fire emissions
770 turned ON, while the sensitivity test for changing the initial emissions and using WRF-Chem
771 show differences of simulations turning smoke emissions on and off. These three sensitivity
772 cases are highlighted in Figure 9 for better comparison.

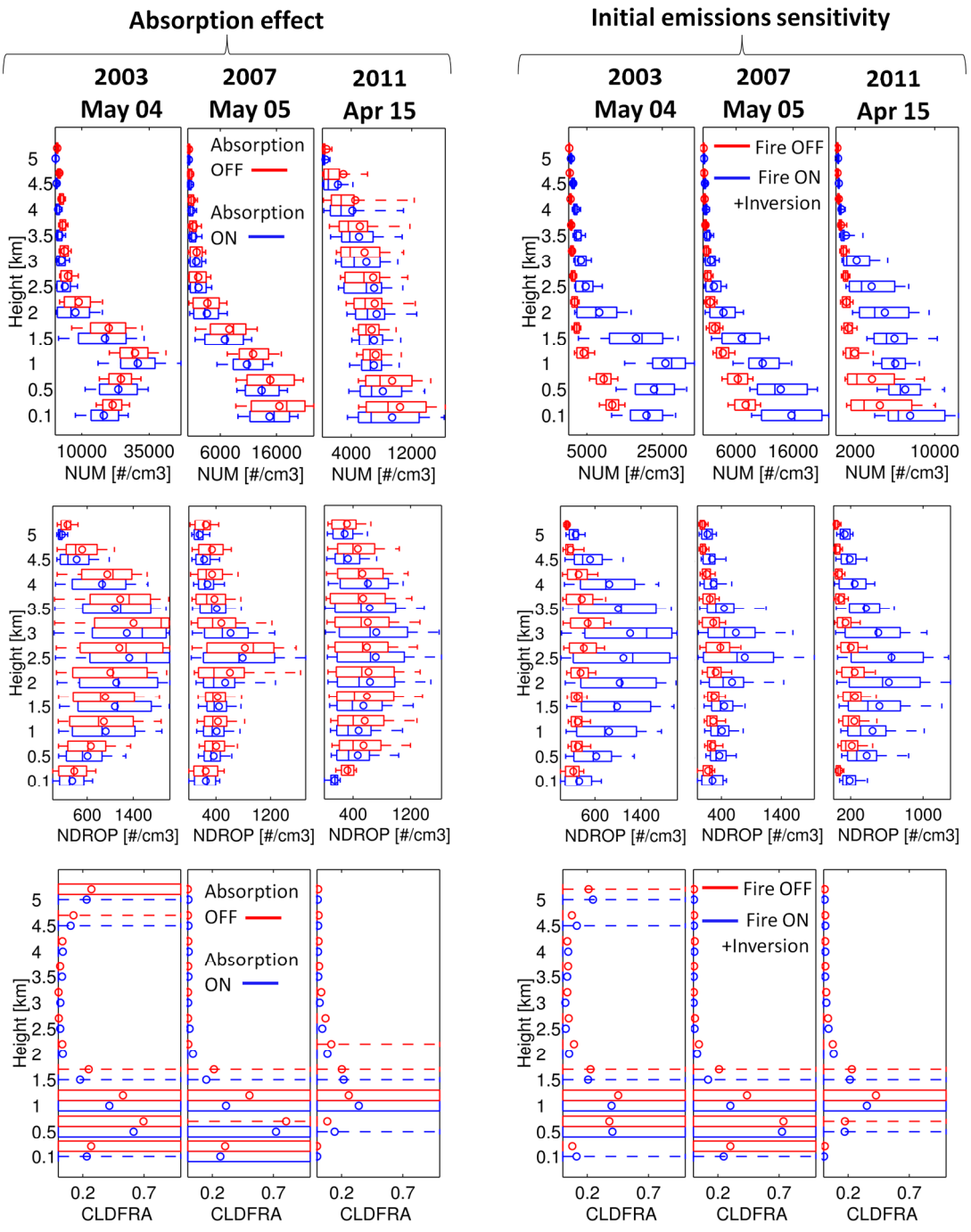

773

774 Figure 11. As Figure 7 for two sensitivity cases, turning off aerosol absorption (left panels) and

775 performing the inversion with a different set of initial biomass burning emissions (right panels).

776 See details of these simulations on the text. The left panels show a comparison of two

777 simulations with biomass burning turned on while the right panels compares simulations with

778 emissions turned on and off.

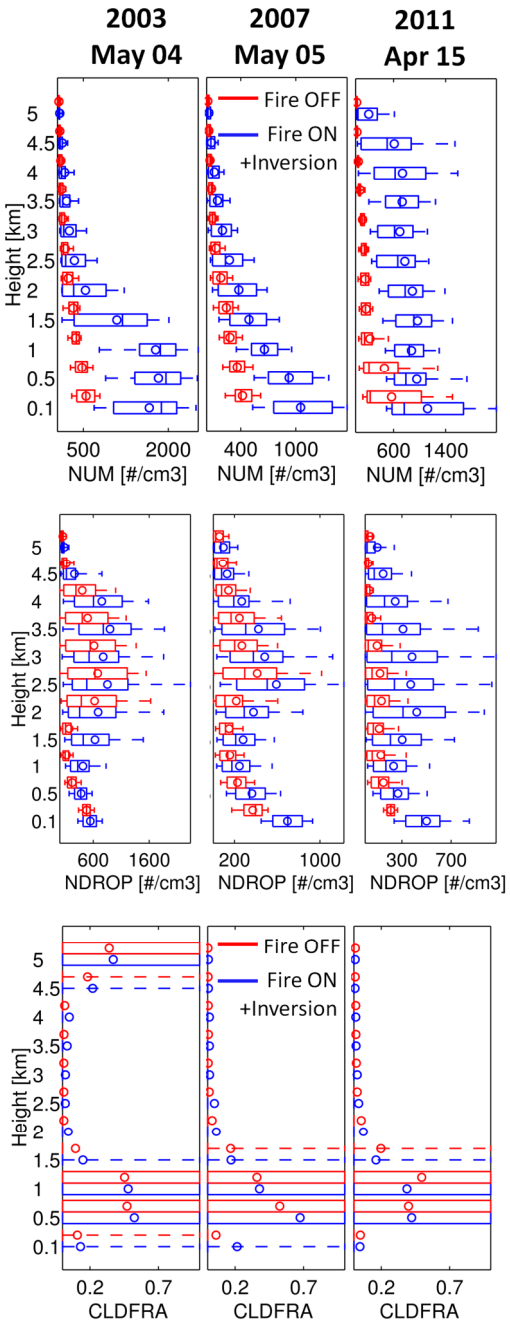

779

780 Figure 12. As Figure 7 but for WRF-Chem simulations. Aerosol number corresponds to the

781 accumulations mode (150-625 µm dry diameter)